



UNIVERSITÀ DI PARMA

ARCHIVIO DELLA RICERCA

University of Parma Research Repository

Influence of the transition width on the magnetocaloric effect across the magnetostructural transition of Heusler alloys

This is the peer reviewed version of the following article:

Original

Influence of the transition width on the magnetocaloric effect across the magnetostructural transition of Heusler alloys / Cugini, Francesco; Porcari, Giacomo; Fabbrici, Simone; Albertini, F.; Solzi, Massimo. - In: PHILOSOPHICAL TRANSACTIONS OF THE ROYAL SOCIETY OF LONDON SERIES A: MATHEMATICAL PHYSICAL AND ENGINEERING SCIENCES. - ISSN 1364-503X. - 374:2074(2016), p. 20150306. [10.1098/rsta.2015.0306]

Availability:

This version is available at: 11381/2806900 since: 2025-04-09T14:25:43Z

Publisher:

Royal Society of London

Published

DOI:10.1098/rsta.2015.0306

Terms of use:

Anyone can freely access the full text of works made available as "Open Access". Works made available

Publisher copyright

note finali coverpage

(Article begins on next page)

02 May 2026

Journal: **PHILOSOPHICAL TRANSACTIONS OF THE ROYAL SOCIETY A**

Article id: **RSTA20150306**

Article Title: **Influence of the transition width on the magnetocaloric effect across the magnetostructural transition of Heusler alloys**

First Author: F. Cugini

Corr. Author(s): F. Albertini

AUTHOR QUERIES – TO BE ANSWERED BY THE CORRESPONDING AUTHOR

As the publishing schedule is strict, please note that this might be the only stage at which you are able to thoroughly review your paper.

Please pay special attention to author names, affiliations and contact details, and figures, tables and their captions.

No changes can be made after publication.

The following queries have arisen during the typesetting of your manuscript. Please answer these queries by marking the required corrections at the appropriate point in the text.

Q1	While the online version of figures 4 and 7 will be in colour, we have been instructed to print the figures in black and white. Please note that if you have explicitly referred to colour in the caption this may affect the legibility of the figures in print.
----	---



Research

Cite this article: Cugini F, Porcari G, Fabbrici S, Albertini F, Solzi M. 2016 Influence of the transition width on the magnetocaloric effect across the magnetostructural transition of Heusler alloys. *Phil. Trans. R. Soc. A* 20150306. <http://dx.doi.org/10.1098/rsta.2015.0306>

Accepted: 9 May 2016

One contribution of 16 to a discussion meeting issue 'Taking the temperature of phase transitions in cool materials'.

Subject Areas:

materials science, solid state physics

Keywords:

magnetocaloric effect, Heusler alloys, magneto-structural transitions, magnetic shape memory materials

Author for correspondence:

F. Albertini


e-mail: franca.albertini@imem.cnr.it

Influence of the transition width on the magnetocaloric effect across the magnetostructural transition of Heusler alloys

F. Cugini^{1,2}, G. Porcari¹, S. Fabbrici², F. Albertini² and M. Solzi¹

¹Department of Physics and Earth Sciences, University of Parma, Parco Area delle Scienze 7/A, 43124 Parma, Italy

²IMEM-CNR Institute, Parco Area delle Scienze 37/A, 43124, Parma, Italy

 FC, 0000-0003-0275-1986; GP, 0000-0002-6960-3681; SF, 0000-0002-8756-0750; FA, 0000-0002-7210-0735; MS, 0000-0002-9912-4534

We report a complete structural and magneto-thermodynamic characterization of four samples of the Heusler alloy Ni-Co-Mn-Ga-In, characterized by similar compositions, critical temperatures and high inverse magnetocaloric effect across their metamagnetic transformation, but different transition widths. The object of this study is precisely the sharpness of the martensitic transformation, which plays a key role in the effective use of materials and which has its origin in both intrinsic and extrinsic effects. The influence of the transition width on the magnetocaloric properties has been evaluated by exploiting a phenomenological model of the transformation built through geometrical considerations on the entropy versus temperature curves. A clear result is that a large temperature span of the transformation is unfavourable to the magnetocaloric performance of a material, reducing both isothermal entropy change and adiabatic temperature change obtainable in a given magnetic field and increasing the value of the maximum field needed to fully induce the transformation. The model, which is based on standard magnetometric and conventional calorimetric measurements, turns out to be a convenient tool for the determination of the optimum values of transformation

temperature span in a trade-off between sheer performance and amplitude of the operating range of a material.

This article is part of the themed issue 'Taking the temperature of phase transitions in cool materials'.

1. Introduction

Over the last two decades, magnetic refrigeration has attracted a great interest as a technological alternative to the conventional gas compression–expansion technique. The finding of suitable magnetocaloric materials, alternative to Gd, with large and reversible magnetocaloric properties, i.e. isothermal entropy change (Δs) and adiabatic temperature change (ΔT_{ad}), for cyclic applications in moderate magnetic fields will play a decisive role to bring this technology into the market [1].

The research in this field was boosted by the introduction in 1997 by Pecharsky and Gschneidner of the 'giant' magnetocaloric material $\text{Gd}_5(\text{SiGe})_4$, showing high Δs at room temperature, associated with a first-order magneto-structural phase transition [2,3]. Since then a great effort has been addressed towards material systems displaying the first-order phase changes, involving a significant latent heat [4–8].

Among them magnetic shape memory Heusler alloys represent a particularly interesting class [9]. They are RE-free, easy-to-prepare and offer large tailoring possibilities. Their interesting phenomenology arises from a martensitic phase transition from a high-temperature cubic phase (austenite) to a low-temperature low-symmetry phase (martensite) that involves a change in both structural and magnetic properties. Remarkably, thanks to the strong discontinuities of the physical properties at the martensitic transformation, caloric effects can be obtained not only by applying magnetic fields but also stress and pressure, enabling multicaloric applications [10–12].

By exploiting suitable compositional changes of $\text{Ni}_{2+x}\text{Mn}_{1+y}\text{X}_{1+z}$ ($X = \text{Ga, In, Sn, Sb}$, $x + y + z = 0$) it has been possible to control the main physical properties of this class of materials and consequently tune the magnetocaloric performances: e.g. critical temperatures, field dependence of the transformation temperature, intensity and nature of the magnetocaloric effect (from direct to inverse) [9]. In particular, a crucial goal of the magnetocaloric research has been modelling the magnetic interactions in martensitic and austenitic phases and increasing the magnetization discontinuity (ΔM) at the transformation [13,14]. In off-stoichiometric Ga-based compounds by changing the relative amount of the constituent elements, it is possible to merge martensitic and Curie temperatures and obtain a direct first-order transformation from ferromagnetic martensite to paramagnetic austenite, giving rise to a direct magnetocaloric effect [6]. On the other hand, In-, Sn- and Sb-compounds show, in suitable stoichiometric ranges, a martensitic transformation between a paramagnetic-like martensite and a ferromagnetic austenite, a feature which makes them known in the literature as 'metamagnetic Heuslers'. In this case, an inverse and remarkable magnetocaloric effect has been obtained [9].

NiCoMnGa-based alloys also belong to the family of metamagnetic Heuslers: stoichiometry controls the critical temperatures, and allows for the realization of materials where the sequence of structural (occurring at the critical temperature T_M) and magnetic (occurring at T_C^M and T_C^A) transitions can be swapped: in Ni-Co-Mn-Ga this means that the martensitic transformation can be realized between ferromagnetic phases, between paramagnetic phases and, most interestingly, between a paramagnetic-like martensite and ferromagnetic austenite [15,16]. Additionally, it was found that partial substitution of Ga with In allows to selectively lower the structural critical temperature while leaving the magnetic critical temperatures almost unaffected [13]. This finding introduces a further degree of freedom in designing the magneto-structural behaviour of these alloys: in particular, it allows to further separate T_M and T_C^A , maximizing the magnetization jump occurring at the transformation. Comparison between quaternary and In-doped quinary compositions allowed to verify that alloys showing higher magnetization jumps displayed also

107 higher structural discontinuities, measured by X-ray diffraction experiments as the relative
108 volume change between the two phases.

109 Although metamagnetic Heusler show high values of inverse magnetocaloric effect (adiabatic
110 temperature changes up to $\Delta T_{\text{ad}} \sim 8 \text{ K}$ in $\mu_0 H = 1.95 \text{ T}$ [17] at the first application of magnetic
111 field) their performances are strongly reduced on subsequent runs of the magnetic field. The
112 hysteretic character of the transition represents a strong drawback for the cyclic use of these
113 materials. It is well assessed that the reversibility of the magnetocaloric effect depends upon two
114 factors: the extent of the hysteresis and the shift in the transition temperature with field [18]. The
115 current research is addressed to systems with low hysteresis and large field dependence of the
116 martensitic transformation temperature, enabling high reversibility rates in moderate magnetic
117 fields (around 1 T). The possible exploitation of minor loops or artificial phase nucleation sites
118 has been proposed; yet, a deeper understanding of thermal and magnetic hysteresis is required
119 to improve materials performances [17,19,20]. Some recent works have been addressed to this
120 [21–23]. Several aspects have to be taken into account both of intrinsic and of extrinsic origin, such
121 as crystalline symmetry and geometric compatibilities of martensite and austenite, local variation
122 of composition, internal stresses, lattice defects, atomic ordering and dynamic properties of the
123 transformation [24–26].

124 On the other hand, not only hysteresis but also the sharpness of the martensitic transformation
125 plays a crucial role in the effective use of materials, and similarly it is due to both intrinsic and
126 extrinsic effects. The full potential of a material can be exploited only if the applied field is large
127 enough to induce the complete transition, being the magnetocaloric effect proportional to the
128 transformed fraction of phase [8].

129 In this paper, we report on four samples of the Heusler alloy Ni-Co-Mn-Ga-In; the samples
130 were chosen with similar compositions, critical temperatures and high inverse magnetocaloric
131 effect across their metamagnetic transformation, but different transition widths. We will provide
132 a complete structural and magneto-thermodynamic characterization of the alloys through in-
133 field calorimetry and evaluate the role of the transition width on the magnetocaloric properties
134 by taking advantage of a phenomenological model of the transformation built through on
135 geometrical consideration on the entropy versus temperature curves.

137 2. Methods

139 Ni-Co-Mn-Ga-In samples were prepared by arc melting the stoichiometric amounts of high-purity
140 elements. To prevent oxidation, a protective Ar atmosphere was established through several Ar-
141 vacuum cycles and pure Ti was melted for 3 min prior every fusion to act as getter of residual
142 oxygen. Melted buttons were turned around and re-melted four times to improve homogeneity;
143 samples were then wrapped in Ta foil and annealed for 72 h at 1173 K in a protective atmosphere,
144 finalized by water quenching. The composition was experimentally determined through energy
145 dispersive spectroscopy (EDS) microanalysis on a Philips 515 scanning electron microscope.

146 Thermomagnetic analysis (TMA) determined the structural and magnetic critical temperatures
147 of the grown samples by measuring the a.c. susceptibility in a purpose-built susceptometer
148 working at 0.5 mT and 500 Hz. Temperature-dependent X-ray diffraction patterns were collected
149 with a Thermo ARL X'tra diffractometer equipped with a solid-state Si(Li) Peltier detector
150 and an environmental chamber. Specific heat measurements were performed with a homemade
151 differential scanning calorimeter (DSC) based on thermoelectric modules [27]. This in-field DSC
152 is able to work in 10^{-5} mbar vacuum between 250 and 420 K and in magnetic fields up to 1.8 T. Its
153 temperature control resolution is $\pm 0.01 \text{ K}$ and the thermal sweep is controlled by a high-power
154 Peltier cell. The calibration was performed by using a single-crystal sapphire sample. The error
155 of specific heat data is estimated to be about 4%. Such error is due to slightly different vacuum
156 conditions between the calibration and consecutive measurements and due to small oscillations
157 of the temperature sweep rate. The reported measurements were carried out with temperature
158 sweeps in heating and cooling at a rate of 2 K min^{-1} , in zero magnetic field and in a magnetic
159 field $\mu_0 H = 1.8 \text{ T}$.

3. Results and discussion

Figure 1 shows the TMA of four Co- and In-doped NiMnGa Heusler alloys of general formula $\text{Ni}_{50-x}\text{Co}_x\text{Mn}_{50-y}(\text{Ga},\text{In})_y$: their measured compositions are reported in table 1, as well as their critical temperatures, measured as the inflection points on the susceptibility curves recorded by TMA. All the samples show a similar transformation between a paramagnetic-like martensite, characterized by a null signal of the susceptibility, and a ferromagnetic austenite, evidenced by the high susceptibility region in the TMA curves. The martensitic Curie temperatures occur well below room temperature, between 170 and 223 K; the transformation temperatures are all above room temperature and in a narrow interval, ranging between 350 K for sample S2 and 388 K for sample S1. The austenitic Curie temperatures, which are mostly influenced by the Co content, occur between 430 K (sample S1) and 476 K (sample S3). Besides these similarities, TMA highlights quite different transformation widths and hysteresis.

In order to evaluate the structural properties, powder X-ray diffraction patterns were collected on each sample in a wide temperature range across the transformation. The powders used for the experiments were heat treated to reduce crystal defects and stresses introduced by grinding.

All samples transform from cubic austenite to tetragonal martensite; the diffraction patterns have been fitted through the LeBail algorithm [28] to extrapolate the lattice parameters of the two phases at various temperatures. In the following, we discuss the results for sample S3, which is representative of the whole series. Figure 2 shows a notable region of the diffraction patterns and their evolution with temperature: the lowering of the austenitic reflections and the onset of the tetragonal martensitic phase are clearly visible. The patterns were collected on cooling from austenite to martensite in the range 453–283 K: the martensitic diffraction peaks become clearly visible below 370 K, and traces of the austenitic phase are detectable at the lowest temperature of the series. Figure 3*a,b* shows the temperature evolution of the martensitic lattice parameters (figure 3*a*) and the tetragonal distortion $c_M/a_M\sqrt{2}$ (figure 3*b*): the tetragonal plane (the a_M lattice parameter) shows almost negligible thermal expansion in the measure range. On the other hand, the tetragonal c_M axis shows a quite strong contraction coming from high-temperature down to 343 K, which is the closest value in the measured series to the cooling martensitic temperature measured by TMA ($T_{A-M} = 350$ K) (figure 1). On further cooling, the c_M axis reverts the trend and increases again to higher values. The anomalous behaviour of the tetragonal axis is evidenced in the evolution of the tetragonal distortion and of the martensitic volume, which show a minimum at the transformation temperature T_{A-M} .

The analysis of the temperature dependence of the lattice parameters allows for the determination of several features useful for characterizing the transformation [13]: besides the tetragonal distortion of the martensitic lattice, described above, the relative volume change $\Delta V/V$ provides a measure of the structural discontinuity between martensite and austenite, while the middle eigenvalue of the transformation matrix λ_2 , defined for the cubic-tetragonal transformation as $\lambda_2 = a_M\sqrt{2}/a_A$, is a good parameter [24] for describing the lattice mismatch at the transformation invariant plane. The calculation of the unit cell volumes and relative changes are reported at figure 3*c,d*. From figure 3*c*, it appears that the two phases have different thermal expansion factors: thus, the relative volume change is not constant over temperature. Additional variability, visible as scattering of the computed quantities in the graphs of figure 3, is generated by the thermal drift of the experimental set-up during the pattern acquisitions and by the error propagation induced by calculations; it is therefore sensible to estimate the mean transformation $\Delta V/V$ by considering the linear fit of the computed values at different temperatures and extrapolating at T_{A-M} . For sample S3, we estimate $\Delta V/V \approx 0.85 \pm 0.05\%$. The same mathematical approach has been followed for the estimation of the mean tetragonal distortion and the λ_2 values.

Table 2 reports the computed values of relative volume discontinuity, $\Delta V/V$, tetragonal distortion, $c_M/a_M\sqrt{2}$ and invariant plane mismatch, $\lambda_2 = a_M\sqrt{2}/a_A$, for the presented samples. The relative volume change is the quantity with the highest variability within the series: the maximum volume discontinuity is $\approx 1.2 \pm 0.1\%$ for sample S2, while the smallest one

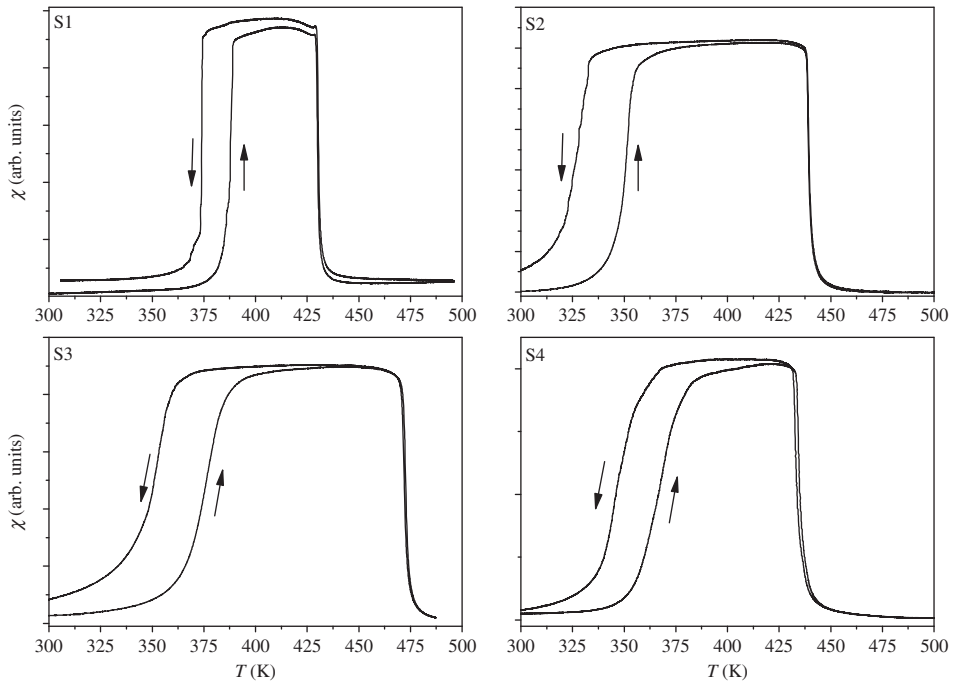


Figure 1. Temperature dependence of the a.c. susceptibility curves. To improve readability only the range 300–500 K is displayed.

Table 1. Compositions measured by EDS are expressed as at.%. The reported error is the standard deviation estimated from the compositional mapping; the lower bound to the error is the instrument uncertainty, $\pm 0.1\%$. Magnetic (T_C^M , T_C^A) and structural (T_{A-M} , T_{M-A}) critical temperatures are estimated as the inflection points of the susceptibility curves.

sample	composition (at.%)					T_C^M (K)	T_C^A (K)	T_{A-M} (K)	T_{M-A} (K)
	Ni	Co	Mn	Ga	In				
S1	42.4 ± 0.2	7.1 ± 0.2	33.0 ± 0.2	15.3 ± 0.2	2.3 ± 0.2	223	430	374	388
S2	41.7 ± 0.2	8.6 ± 0.3	32.3 ± 0.4	14.1 ± 0.2	3.3 ± 0.2	205	440	326	351
S3	40 ± 0.3	10.8 ± 0.2	31.4 ± 0.2	16.5 ± 0.2	1.4 ± 0.2	170	473	350	375
S4	41.7 ± 0.2	8.1 ± 0.3	33.3 ± 0.4	13.8 ± 0.3	3.2 ± 0.2	198	433	346	367

is $\approx 0.6 \pm 0.1\%$ for sample S1. The values of tetragonal distortion and transformation matrix eigenvalue show a much smaller variance. A similar trend as the one observed for the volume discontinuity is however established: sample S1 shows the least tetragonal distortion and the highest compatibility factor (λ_2 is the closest to unity of the series), while sample S2 shows the highest tetragonal distortion and the lowest value of λ_2 .

The thermodynamic and thermomagnetic properties of the four presented samples are explored by measuring their specific heat under magnetic field across the martensitic transformation. In-field differential scanning calorimetry (DSC) offers a large amount of information concerning the thermodynamic and magnetocaloric features of materials exploiting first-order transitions [29]. Figure 4 shows the specific heat of the samples measured with temperature sweeps on heating and cooling in zero and in a 1.8 T applied magnetic field. The specific heat of martensitic and austenitic phases, before and after the transition, is nearly the

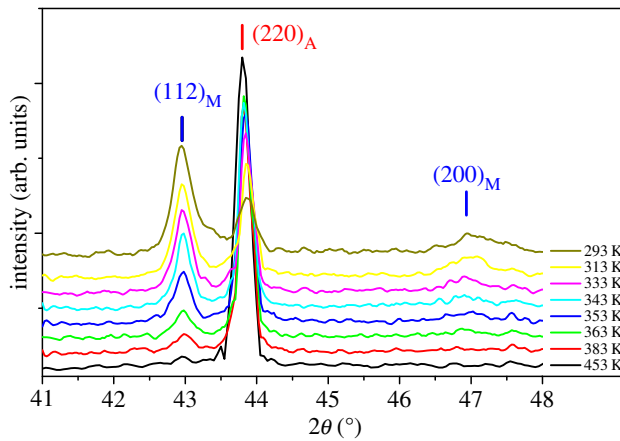


Figure 2. Temperature evolution of the diffraction patterns collected across the transformation temperature. A narrow 2θ range has been displayed to highlight the temperature evolution of the indexed reflections of austenite (A subscript) and martensite (M subscript). (Online version in colour.)

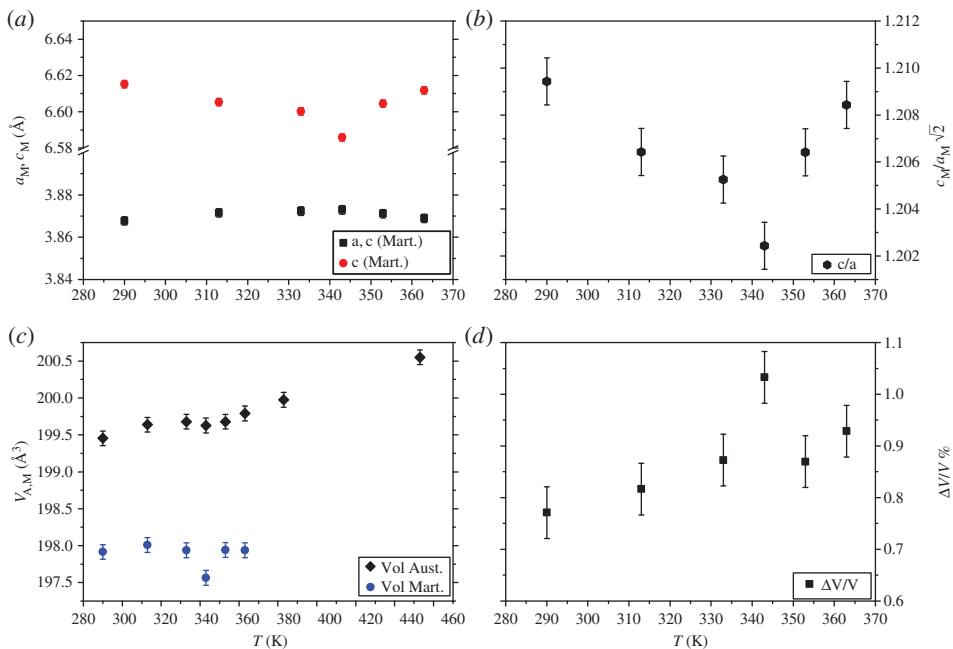


Figure 3. Temperature evolution of (a) the martensitic lattice parameters; (b) the tetragonal distortion $c_M/a_M\sqrt{2}$; (c) the austenitic and martensitic cell volumes and (d) the relative volume change $\Delta V/V$. (Online version in colour.)

same for the four samples ($c_{p_{\text{mart}}} \approx 480 \text{ J kg}^{-1} \text{ K}^{-1}$ at 300 K and $c_{p_{\text{aust}}} \approx 570 \text{ J kg}^{-1} \text{ K}^{-1}$ at 400 K), and it shows a slow variation with temperature. At the transition temperature, the presence of peaks in the specific heat confirms that this magnetic transition is of first order; the heating and cooling peaks are separated by the transformation hysteresis, while the magnetic field, as expected for inverse MCE alloys, promotes the high-temperature magnetic phase thus shifting the transformations to lower temperatures. From the shift of the heat flow peaks, we can deduce the values of $dT/\mu_0 dH$. The values, calculated for the transition on heating and on cooling,

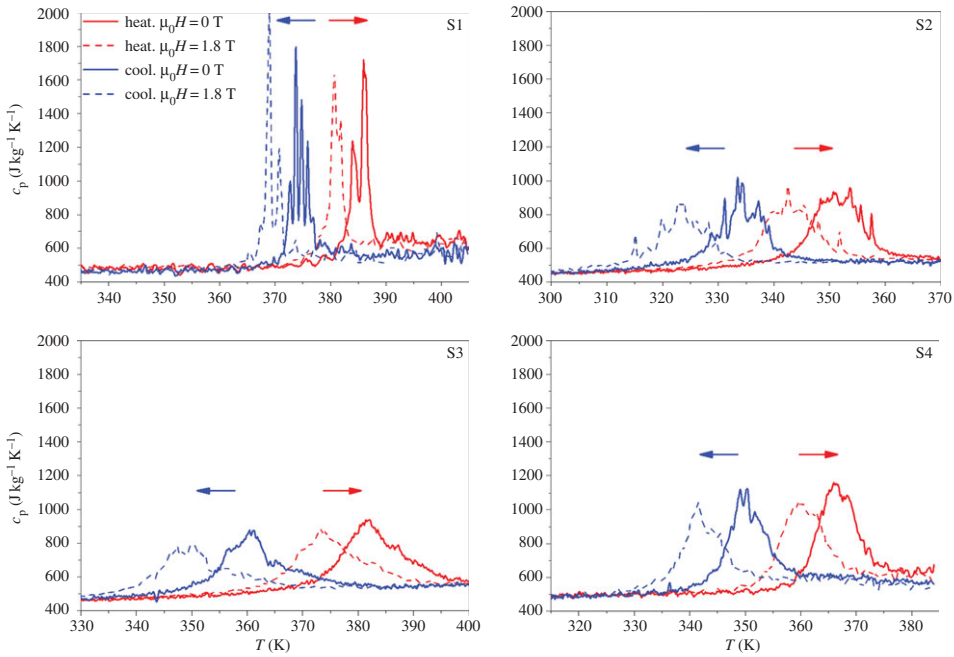


Figure 4. Specific heat curves of the four samples in $\mu_0 H = 0$ T (solid lines) and 1.8 T (dashed lines) measured with temperature sweeps on heating (red lines, right arrow) and on cooling (blue lines, left arrow). (Online version in colour.)

Table 2. Mean values of the relative volume change ($\Delta V/V$), tetragonal distortion of the martensitic cell (t), middle eigenvalue of the transformation matrix (λ_2). The means were calculated at the transformation temperature from the linear fits, as described in the text.

sample	volume discontinuity $\Delta V/V$ %	tetragonal distortion $t = c_M/a_M\sqrt{2}$	middle eigenvalue $\lambda_2 = a_M\sqrt{2}/a_A$
S1	0.6 ± 0.1	1.200 ± 0.005	0.940 ± 0.002
S2	1.2 ± 0.1	1.210 ± 0.005	0.933 ± 0.002
S3	0.85 ± 0.05	1.205 ± 0.005	0.936 ± 0.001
S4	0.88 ± 0.025	1.202 ± 0.005	0.937 ± 0.001

are reported in table 3. In all the samples, the $dT/\mu_0 dH$ across the cooling transformation is higher than that in the heating branch. This confirms the already reported behaviour [14,30] according to which the magnetic field shifts more the transformation temperature on cooling due to the larger magnetization jump. Observing the temperature of peaks in the cooling and heating measurements, we can deduce also the values of the thermal hysteresis (reported in table 3), which characterize the first-order transition. The different field sensitivity of the cooling and heating critical temperatures affects also the thermal hysteresis: the in-field hysteresis is larger than the zero-field one.

The peaks' shape, width and height are different for every samples and do not seem to be correlated with the stoichiometric composition. The area under the peaks corresponds to the latent heat (L) of the fully transformed phase, which can be calculated by integrating the specific heat data after subtraction of the baseline ($c_{p,\text{baseline}}$) between the start and finish temperature of the

Table 3. Characteristics of the first-order transition of the four samples as obtained from DSC data: transition temperature in zero applied magnetic field on heating T_p , transition width (full width at half maximum (FWHM) of the specific heat peak at zero magnetic field on heating), latent heat of the transition in zero applied field on heating L , magnetic field dependence of the transition temperature $dT/\mu_0 dH$ on heating and cooling, thermal hysteresis in zero and applied magnetic field (Hyst.).

sample	T_p (K)	FWHM (K)	L (J kg ⁻¹)	$dT/\mu_0 dH$ heating (K T ⁻¹)	$dT/\mu_0 dH$ cooling (K T ⁻¹)	Hyst. $\mu_0 H = 0$ T (K)	Hyst. $\mu_0 H = 1.8$ T (K)
S1	385.0 ± 0.3	3.1 ± 0.3	2600 ± 80	-2.4 ± 0.6	-2.7 ± 0.6	10.4 ± 0.6	11.6 ± 0.6
S2	351.9 ± 0.5	10.0 ± 0.8	4700 ± 140	-4.6 ± 1.0	-5.9 ± 1.0	16.7 ± 1.0	19.1 ± 1.0
S3	381.4 ± 0.5	11.0 ± 1.0	4450 ± 130	-4.5 ± 1.0	-5.9 ± 1.0	21.5 ± 1.0	24.0 ± 1.0
S4	366.6 ± 0.5	7.7 ± 0.7	5150 ± 150	-3.5 ± 1.0	-4.3 ± 1.0	16.9 ± 1.0	18.4 ± 1.0

transformation (T_s and T_f):

$$L(H) = \int_{T_s}^{T_f} (c_p(T', H) - c_{p,\text{baseline}}(T')) dT' \quad (3.1)$$

The calculated latent heat values are comparable with those measured in samples with similar composition [14]. Both the application of magnetic field and the shift to lower temperatures of the transformation observed in the cooling curves result in a sizeable reduction of L . The strong action of the magnetic field on the latent heat was already observed in Ni-Mn-Co-Ga-In [14]. The absence of In in the quaternary alloys reduces this effect, which disappears in the parent Ni₂MnGa alloy, showing a ferro-ferro martensitic transformation [14].

The comparison between zero and in-field specific heat data gives the possibility to obtain a complete MCE characterization of the samples. The integration of the calorimetry data provides the entropy-temperature curves across the transition at different magnetic fields:

$$s(T, H) - s(T_0) = \int_{T_0}^T \frac{c_p(T', H)}{T'} dT' \quad (3.2)$$

The adiabatic temperature change $\Delta T_{\text{ad}}(T)$ and the isothermal entropy change $\Delta s(T)$ can be deduced from the obtained $s - T$ curves. The errors correlated with this numerical manipulation of specific heat data can be estimated following the discussion of Porcari *et al.* [27] and Pecharsky & Gschneidner [31]. The temperature behaviour of $\Delta s(T)$ and $\Delta T_{\text{ad}}(T)$ for a $\mu_0 \Delta H$ of 1.8 T are reported in figure 5. The results of samples S2 and S4 have been compared with the $\Delta s(T)$ obtained by magnetic measurements using the Maxwell relation and with the $\Delta T_{\text{ad}}(T)$ directly measured with a probe based on a Cernox temperature sensor [32]. The results obtained from the different techniques, provided that they have been used with the proper measurement protocol and on strictly the same sample, turn out to be consistent, as already demonstrated in [27]. The peak values Δs_{peak} and $\Delta T_{\text{ad,peak}}$ for a magnetic field span $\mu_0 \Delta H = 1.8$ T across the transformation on heating are shown in table 4. The $\Delta T_{\text{ad,peak}}$ values reported in this paper are the highest of all the Ga-based Heuslers [14,27,33,34], reaching almost 2 K T⁻¹ for sample S2. For all the samples, the measured Δs_{peak} results lower than the maximum entropy change of the fully induced phase, estimated from latent heat $\Delta s_{\text{full}} \approx L/T_p$. This means that a magnetic field of 1.8 T does not fully induce the transformation in those samples. We can observe in table 4 that there is no close relationship between the Δs_{peak} and the Δs_{full} values: for instance, S4 has the biggest $\Delta s_{\text{full}} = 14$ J kg⁻¹ K⁻¹ among the four samples but it shows a Δs_{peak} lower than that of S2. This fact underlines that further quantities characterizing the transitions play a role to determine the $\Delta s(T)$ and $\Delta T_{\text{ad}}(T)$ of real materials. A large Δs_{full} , which on the basis of the Clausius-Clapeyron relation is proportional to the magnetization difference between the two phases, is not enough to ensure a large Δs_{peak} exploitable in thermomagnetic cycles. There is instead a correlation between $\Delta T_{\text{ad,peak}}$ and $(dT/\mu_0 dH)$, however also in this case none of the samples reaches the maximum expected value of ΔT_{ad} , calculated as $\Delta H \cdot (dT/dH)$ (table 4).

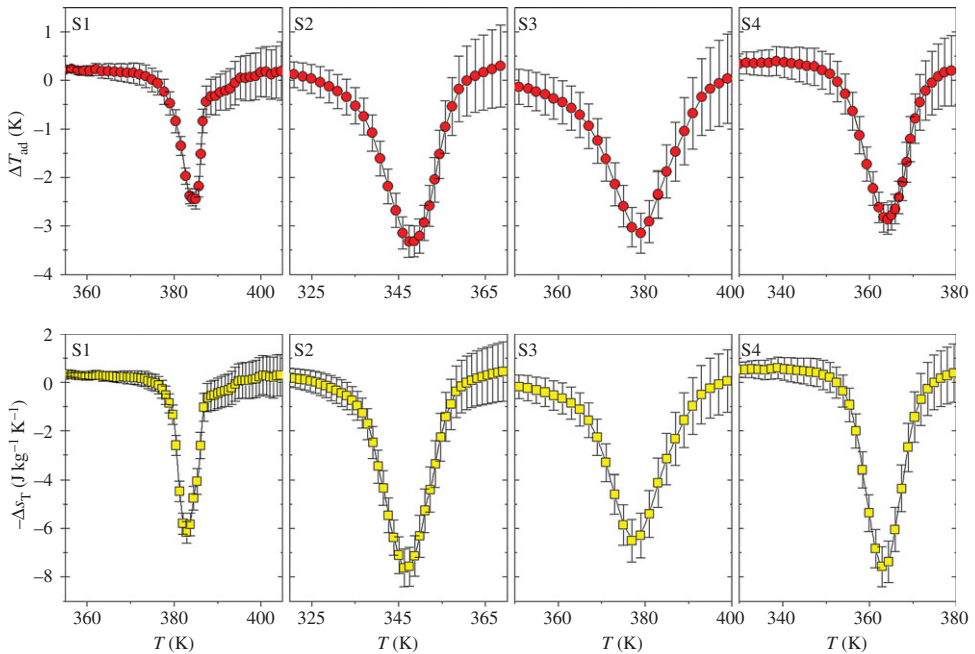


Figure 5. $\Delta T_{ad}(T)$ (circles) and $\Delta s(T)$ (squares) for a $\mu_0 \Delta H = 1.8$ T calculated from DSC data on heating. (Online version in colour.)

Table 4. Peak values of the isothermal entropy variation Δs_{peak} and of the adiabatic temperature change $\Delta T_{ad,peak}$ in a field span of 1.8 T calculated from specific heat data. Comparison of these values with the expected entropy changes of the fully induced transition $\Delta s_{full} \approx L/T_p$ and the maximum achievable adiabatic temperature change $\Delta T_{max} = \Delta H \cdot (dT/dH)$. The adiabatic temperature change ΔT_{calc} is calculated using equation (3.8) from data reported in table 3.

sample	Δs_{peak} ($J kg^{-1} K^{-1}$)	Δs_{full} ($J kg^{-1} K^{-1}$)	$\Delta s_{peak}/\Delta s_{full}$ (%)	$\Delta T_{ad,peak}$ (K)	ΔT_{max} (K)	$\Delta T_{peak}/\Delta T_{max}$ (%)	ΔT_{calc} (K)
S1	6.2 ± 0.5	6.8	91	-2.5 ± 0.2	4.3	58	2.7
S2	7.7 ± 0.8	13.4	57	-3.3 ± 0.3	8.3	40	4.1
S3	6.5 ± 0.9	11.7	56	-3.1 ± 0.4	8.1	38	3.7
S4	7.5 ± 0.8	14	54	-2.9 ± 0.3	6.3	46	3.6

The key to understand the behaviour of these materials is the transformation width (W): we can observe in figure 4 that for all the samples the transition occurs over a large temperature range rather than at a well-defined temperature, as expected in principle for a first-order transition. We estimated W from the calorimetric measurements as the FWHM of the transformation peaks (table 3), because it is difficult to exactly determine the initial and final temperature of the transition. The quantity W assumes a relevant role in determining both Δs and ΔT_{ad} . We can observe that S1, which has the narrowest W , is the sample in which the 1.8 T magnetic field manages to transform almost all the phase ($\Delta s_{peak}/\Delta s_{full} = 91\%$). At the same time, this sample has the highest ratio between the measured ΔT_{peak} and the maximum exploitable ΔT_{ad} , as deduced from the relation $\Delta T_{max} = \Delta H (dT/dH)$.

As for thermal and magnetic hysteresis, several features contribute to the smearing of the transformation over temperature, both extrinsic and intrinsic to the material. Lattice mismatch (e.g. λ_2) and volume differences $\Delta V/V$ between the two phases contribute to the total free

energy with an elastic strain energy term that plays a major role in broadening the transition and in determining the two-phase stability regions. Coherently, among the measured samples, sample S1, which shows a less pronounced discontinuity of the structural parameters at the transformation (table 2), displays a smaller transformation width (i.e. $W = 3.1 \pm 0.3$ K). However, a direct correlation between intrinsic structural features and transition width cannot be drawn for all the samples, highlighting the crucial role of extrinsic properties in giving rise to variations of the effective local transition temperature.

The compositional inhomogeneity, caused either by improper melting or by phase splitting due to solubility limits of the various elements in the alloy, can be one of the most important contributions. Compositional mapping performed through EDS analysis shows that compositional fluctuations are present in all samples, mainly involving Mn: the composition errors reported in table 1 are the propagation of the standard deviations calculated for all elements with the experimental error of EDS technique, which is in our case ± 0.1 at.%. Uncertainties on Mn top 0.4 at%, while the other elements show much lower deviations, in some cases comparable to the experimental error of EDS. These values, although numerically limited, can be significant in these alloys, where variations of 1 at.% on Mn can in some cases shift the martensitic critical temperature for tens of degrees [15].

Besides compositional inhomogeneities, microstructural features such as defects and grain boundaries, strongly influence the martensitic transformation process that proceeds through nucleation and growth of one phase into the other following an avalanche criticality type of path [17]. Further analysis specifically targeted to these aspects are needed to improve the comprehension of the phenomenon, aiming at a better exploitation of magnetocaloric materials.

In order to understand the role that each thermodynamic and thermomagnetic parameter, characterizing the transition, plays in determining the MCE features, a simple geometrical model is constructed in the $s - T$ plane. A similar model, based on magnetization data, has been introduced in [33] in order to correlate the isothermal (Δs) and adiabatic (ΔT_{ad}) features of the magnetocaloric effect; in this paper, we generalize its construction to take into account also the transformation width.

The model is built drawing the tangent lines at the inflection points of the two entropy curves across the transition, both in zero-field and under applied magnetic field, and the tangent lines at the entropy curves below and above the transition region (figure 6a). In this way, the area in the $s - T$ plane where the MCE is significant looks like a parallelogram. This model physically means that we are considering a linear variation of the phase fraction, the order parameter of the process, over a temperature range W centred at the peak temperature T_p of $c_p(T)$ curve. Figure 6b shows the comparison between the measured specific heat data of sample S2 and the model constructed on such data. The specific heat peaks are approximated by a rectangular shape, which after integration gives rise to the linear trend of the entropy curves at the transition. The rectangle width, W , is determined by the latent heat, which must remain the same obtained from the specific heat data, and by the height of the specific heat peak, calculated as the peak value of a Gaussian best fit of the experimental curve. The temperature dependence of the specific heat below and above the transition is considered to be linear and the entropy curves of the austenitic phase with and without magnetic field are assumed to be overlapping: the effect of applied magnetic field on the austenitic phase, where a direct MCE contribution is expected, turns out to be negligible. Both positive ΔT_{ad} and negative Δs contributions on the high-temperature peak-tails of the transformation, reported in figure 5 for all the samples, are experimentally observed but below the experimental error. Therefore, the latent heat, represented as the segment DB' in figure 6c, is assumed to be the same in zero and applied magnetic field. Although this approximation might seem far from reality, a possible field dependence of latent heat (leading to the $s(T)$ curves not overlapping in the austenitic range) would not affect the determination of peak values of both ΔT_{ad} and Δs : by model construction peak values are realized before the in-field austenitic line starts. The only effect of the magnetic field is to shift the transition temperature T_p to lower temperature. For clarity reasons, we apply this construction on the entropy curves in heating, only. Curves in cooling and the effects due to thermal hysteresis

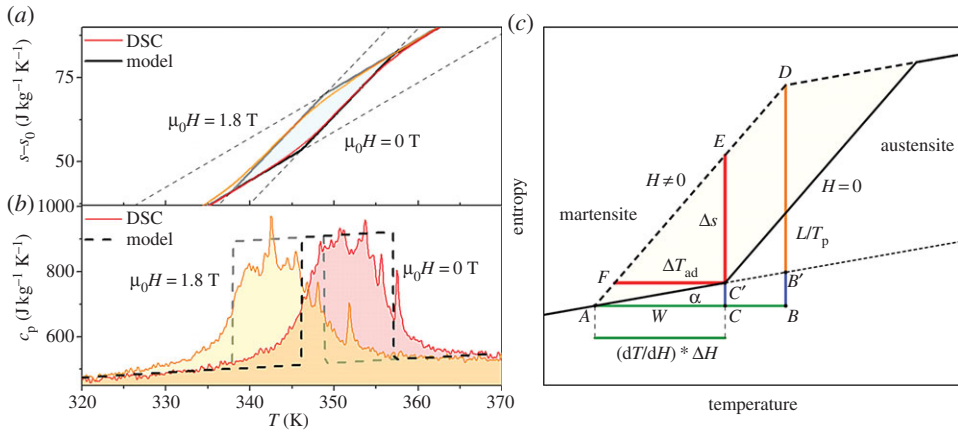


Figure 6. (a) Sketch of the proposed model superimposed to the $s(T)$ curves calculated from DSC data on heating for $\mu_0 H = 0$ and 1.8 T. (b) Comparison between the measured specific heat data and the considered model of the transition. (c) Geometrical constructions based on the model in order to correlate the main parameters of the first order transition (see text for details). (Online version in colour.)

can be introduced too, as it was done by Gottschall *et al.* [26], but this is outside the purpose of this paper.

In this simplified model, five fundamental parameters are enough to describe the transition: the temperature of the transition peak in zero applied magnetic field (T_p), the total latent heat of the transition (λ), the shift of the transition temperature due to the applied magnetic field $\Delta H \cdot (dT/dH)$, the transition width (W) and the specific heat value of the martensitic phase before the transition ($c_{p_{\text{mart}}}$). Thanks to some geometrical proportions (figure 6c), considering the triangles ABD , ACE and $FC'E$, we can link the magnetocaloric features at the transition, ΔT_{ad} and Δs , to these five parameters:

$$\left(\frac{dT}{dH} \Delta H \right) : \Delta T_{\text{ad}} = (\Delta s + CC') : \Delta s \quad (3.3)$$

and

$$W : \Delta T_{\text{ad}} = \left(\frac{L}{T_p} + BB' \right) : \Delta s. \quad (3.4)$$

The segments CC' and BB' depend on the entropy rate before the transition and can be approximated as

$$BB' = AB \tan \alpha \approx AB \frac{c_{p_{\text{mart}}}}{T_p} = W \frac{c_{p_{\text{mart}}}}{T_p} \quad (3.5)$$

and

$$CC' = AC \tan \alpha \approx AC \frac{c_{p_{\text{mart}}}}{T_p} = \frac{dT}{dH} \Delta H \frac{c_{p_{\text{mart}}}}{T_p}. \quad (3.6)$$

The validity of equation (3.3) for real materials was demonstrated in Porcari *et al.* [27] by comparing the ΔT_{ad} values obtained from (3.3) and those directly measured and derived from in-field specific heat data. The proportions (3.3) and (3.4) are strictly valid only for purely first-order systems and when the field-induced transition shift is smaller than the transformation width [34]: all the samples presented in this paper comply with these restrictions.

By inserting (3.5) and (3.6) in (3.3) and (3.4), we obtain:

$$\Delta s_{\text{peak}} = \frac{((dT/dH)\Delta H)L}{T_p W} \quad (3.7)$$

and

$$\Delta T_{\text{ad,peak}} = \frac{((dT/dH)\Delta H)L}{L + Wc_{p_{\text{mart}}}}. \quad (3.8)$$

By combining equations (3.7) and (3.8), it is possible to correlate Δs_{peak} and $\Delta T_{\text{ad,peak}}$

$$\Delta T_{\text{ad,peak}} = \frac{\Delta s_{\text{peak}}}{L/W + c_{p_{\text{mart}}}}. \quad (3.9)$$

One can appreciate how equation (3.9) deviates from previous derivations on the same matter [35]. The reason for such difference originates from the substantially different approximations employed to describe the first-order transformation: we must remark that the derivation appearing in Pecharsky *et al.* is obtained outside the range of validity of the present model, i.e. by assuming idealized sharp transitions ($W = 0$) where the application of the magnetic field is sufficient to complete the transformation, while in this paper we are dealing with partial phase transformations and finite transition ranges. The denominator of equation (3.9) represents an *effective* specific heat inside the transition region, as it is shown in figure 6b, with a factor (L/W) taking into account a contribution of the latent heat that is spread over the whole temperature range of the transition.

Equations (3.7) and (3.8) can be used to estimate the MC features of materials from standard magnetometric and conventional zero-field DSC measurements. The only required parameters to perform the calculation are the specific heat before the transition, the latent heat of the transformation in zero applied field, the peak temperature of the transition, its span width and its change with the applied magnetic field. In table 4, we compare the ΔT_{ad} calculated using equation (3.8) and those obtained from in-field specific heat data. The calculated values show the same trend of the measured ones but they turn out to be overestimated by about 20%. This overestimation is due to the difference between the smoother trend of the experimental entropy curves when compared with the series of line segments of our geometrical model.

Equations (3.7) and (3.8) also give some simple indication on how the various parameters affect the Δs_{peak} and $\Delta T_{\text{ad,peak}}$ values. The first aspect we notice is that higher values of (dT/dH) and L increase both Δs_{peak} and $\Delta T_{\text{ad,peak}}$. The former has a primary role in determining the $\Delta T_{\text{ad,peak}}$ and it represents its upper limit when the product $W \cdot c_{p_{\text{mart}}}$ tends to zero. Regarding instead Δs_{peak} , it reaches its maximum value, limited by the entropy variation of the fully induced phase L/T_p , when the ratio $(dT/dH)/W$ tends to 1. For a lower width of the transition, this model is no longer valid: anyhow, the value of Δs_{peak} cannot grow more and it is expected to remain constant over a finite temperature range. On the contrary, we can observe that an enlargement of the transition width always decreases both the Δs_{peak} and $\Delta T_{\text{ad,peak}}$ values.

These general considerations can be visualized in figure 7. In figure 7a, a series of possible s - T diagrams is represented differing for the transition width W . All the other parameters ($dT/\mu_0 dH, T_p, c_p, L$) are kept constant and equal to those of sample S2. Figure 7b,c reports the variations of $\Delta s(T)$ and $\Delta T_{\text{ad}}(T)$ curves on changing the W value. As discussed above, we can observe that Δs reaches its upper limit when $W = \Delta H \cdot (dT/dH)$ ($=8.3\text{K}$, in this case), while ΔT_{ad} continues to grow for W tending to zero. It is evident indeed that the transition width W plays a key role in changing the Δs_{peak} and $\Delta T_{\text{ad,peak}}$ values as compared to their upper limit: L/T_p and $\Delta T_{\text{max}} = \Delta H \cdot (dT/dH)$, respectively.

As a general consideration aimed at future materials' design, the sole reduction of W should not be the main goal of research: in fact, W acts also on the width of the $\Delta s(T)$ and $\Delta T_{\text{ad}}(T)$, enlarging the area where the MCE is sizable and can thus be exploited in thermodynamic cycles. A guideline for this analysis comes from a careful consideration of the denominator in equation (3.8). Following a straightforward mathematical manipulation, one can also rewrite

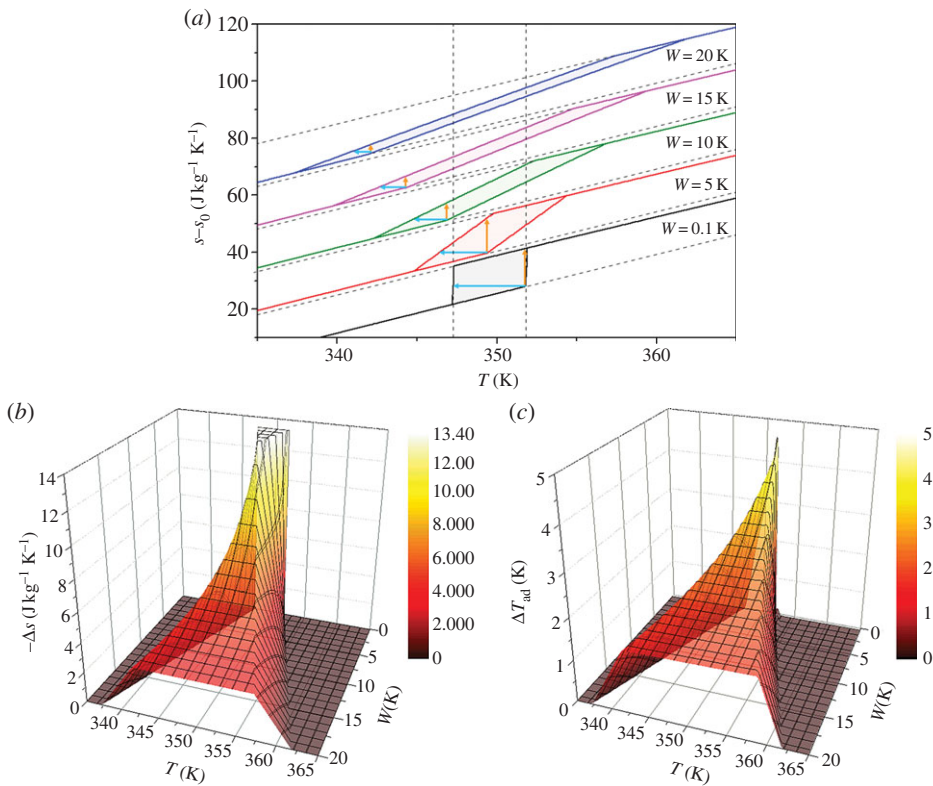


Figure 7. (a) Simulation of different $s(T)$ diagrams on varying the width of the transition temperature span; ΔT_{ad} and Δs are pointed out with blue and orange arrows. (b), (c) Variation of the $\Delta T_{ad}(T)$ and $\Delta s(T)$ as a function of the transition width W , Q1 calculated using the geometrical model. (Online version in colour.)

equation (3.8) as

$$\Delta T_{ad,peak} = \frac{\Delta T_{ad,max}}{1 + Wc_{p,mart}/L'} \quad (3.10)$$

where $\Delta T_{ad,peak}$ is evidenced the combined effect of quantities W and L to determine the $\Delta T_{ad,peak}$ value. Considering that $c_{p,mart}$ is almost constant for all the samples of this series, we deduce from equation (3.10) that a large latent heat allows to keep a relevant $\Delta T_{ad,peak}$ value even in the case of a non-negligible transition width. This statement is valid if the $dT/\mu_0 dH$ is kept constant. Instead, it was observed that for some materials, like for the Fe_2P -based compounds, a larger latent heat decreases the $\Delta T_{ad,peak}$, due to its significant effect on $dT/\mu_0 dH$ [36]. As an example, for sample S1 $L = 2600 \text{ J Kg}^{-1}$ and the relatively small $W = 3.1 \text{ K}$ corresponds to $\Delta T_{ad,peak} = 2.7 \text{ K}$, while for sample S4 it is $L = 5150 \text{ J Kg}$ and, in spite of a larger width $W = 7.7 \text{ K}$, from equation (3.10) it results $\Delta T_{ad,peak} = 3.7 \text{ K}$.

In practical terms, higher values of transformation width, and thus, higher working ranges, can be tolerated without excessive decrease of $\Delta T_{ad,peak}$ and Δs_{peak} as long as high transformation latent heat is obtained.

4. Conclusion

In this contribution, we have presented a thorough calorimetric and structural characterization on four samples of the Heusler alloy Ni-Co-Mn-Ga-In. The studied materials show high values of inverse magnetocaloric effect, triggered by magnetic field in the surroundings of their martensitic

690 transformation temperatures: compared to the other members of the Co- and In-doped Ni-Mn-
691 Ga alloys up to now reported in the literature, we have measured the highest values of adiabatic
692 temperature change (up to almost 2 K/T).

693 The presented samples display similar compositions and magneto-structural phenomenology,
694 yet their martensitic transformations realize in different temperature spans. The different
695 transformation width has to be ascribed to both intrinsic (e.g. structural discontinuity between
696 martensite and austenite) and extrinsic reasons (e.g. samples inhomogeneities, defects, grain
697 boundaries).

698 The role of the transformation broadening on the magnetocaloric properties has been
699 investigated by developing a geometrical model, which traces the transformation coordinates
700 on the entropy–temperature plane. The model is readily applicable, as it relies on standard
701 magnetometric and conventional DSC measurements.

702 It is found that the transition width is always detrimental to the magnetocaloric performances
703 of a material, reducing the amount of both isothermal entropy change and adiabatic temperature
704 change obtainable in a given magnetic field and increasing the value of the maximum field needed
705 to fully induce the transformation; yet, the presented model is a convenient tool for estimating the
706 effects of the transition width on the magnetocaloric properties, allowing for the determination
707 of the optimum values of transformation width in a trade-off between sheer performance and
708 amplitude of the operating range of a material.

709 **Authors' contributions.** All the authors contributed to the data analysis and helped draft and revise the manuscript.
710 F.C. and G.P. performed the calorimetric characterization and developed the geometrical model. S.F.
711 synthesized the samples and performed the TMA measures and the temperature-dependent X-ray diffraction
712 experiments. F.A. and M.S. motivated the study and supervised the research activity. All authors gave final
713 approval for publication.

714 **Competing interests.** The authors declare no competing interests.

715 **Funding.** F.C. thanks Fondazione Cariparma for financial support.

716 **Acknowledgements.** The authors acknowledge the contribution of Dr Davide Calestani (IMEM-CNR) and
717 Dr Tiziano Rimoldi (University of Parma) for their contributions to the experimental characterization
718 (composition measurements).

721 References

- 723 1. Kitanovski A, Tušek J, Tomc U, Plaznik U, Ožbolt M, Poredoš A. 2015 *Magnetocaloric energy*
724 *conversion, green energy and technology*. Switzerland: Springer International Publishing.
- 725 2. Pecharsky K, Gschneidner Jr KA. 1997 Giant magnetocaloric effect in $Gd_5(Si_2Ge_2)$. *Phys. Rev.*
726 *Lett.* **78**, 4494–4497. (doi:10.1103/PhysRevLett.78.4494)
- 727 3. Pecharsky VK, Gschneidner Jr KA. 1997 Tunable magnetic regenerator alloys with a giant
728 magnetocaloric effect for magnetic refrigeration from ~ 20 to ~ 290 K. *Appl. Phys. Lett.* **70**,
729 3299–3302. (doi:10.1063/1.119206)
- 730 4. Tegus O, Brück E, Buschow KHJ, de Boer FR. 2002 Transition-metal-based magnetic
731 refrigerants for room-temperature applications. *Nature* **415**, 150–152. (doi:10.1038/415150a)
- 732 5. Wada H, Tanabe Y. 2001 Giant magnetocaloric effect of $MnAs_{1-x}Sb_x$. *Appl. Phys. Lett.* **79**,
733 3302–3304. (doi:10.1063/1.1419048)
- 734 6. Pareti L, Solzi M, Albertini F, Paoluzi A. 2003 Giant entropy change at the co-occurrence of
735 structural and magnetic transitions in the $Ni_{2.19}Mn_{0.81}Ga$ Heusler alloy. *Eur. Phys. J. B* **32**,
736 303–307. (doi:10.1140/epjb/e2003-00102-y)
- 737 7. Krenke T, Duman E, Acet M, Wassermann EF, Moya X, Manosa L, Planes A. 2005
738 Inverse magnetocaloric effect in ferromagnetic Ni-Mn-Sn alloys. *Nat. Mater.* **4**, 450–454.
739 (doi:10.1038/nmat1395)
- 740 8. Liu J, Gottschall T, Skokov KP, Moore JD, Gutfleisch O. 2012 Giant magnetocaloric effect
741 driven by structural transitions. *Nat. Mater.* **11**, 620–626. (doi:10.1038/nmat3334)
- 742 9. Acet M, Mañosa L, Planes A. 2001 Magnetic-field-induced effects in martensitic Heusler-based
magnetic shape memory alloys. In *Handbook of magnetic materials 19* (ed. KHJ Buschow), ch. 4,
pp. 231–289. Amsterdam, The Netherlands: Elsevier.

- 743 10. Moya X, Kar-Narayan S, Mathur ND. 2014 Caloric materials near ferroic phase transitions. *Nat. Mater.* **13**, 439–450. (doi:10.1038/nmat3951)
- 744
- 745 11. Mañosa L, González-Alonso D, Planes A, Bonnot E, Barrio M, Tamarit JL, Aksoy S, Acet M.
- 746 2010 Giant solid-state barocaloric effect in the Ni-Mn-In magnetic shape-memory alloy. *Nat.*
- 747 *Mater* **9**, 478–481. (doi:10.1038/nmat2731)
- 748 12. Fahler S *et al.* 2012 Caloric effects in ferroic materials: new concepts for cooling. *Adv. Eng.*
- 749 *Mater.* **14**, 10–19. (doi:10.1002/adem.201100178)
- 750 13. Albertini F *et al.* 2011 Reverse magnetostructural transitions by CO and in doping nimnga
- 751 alloys: structural, magnetic, and magnetoelastic properties. In *Advances in magnetic shape*
- 752 *memory materials*, vol. 684 (ed. VA Chernenko), pp. 149–161. Materials Science Forum. Zurich,
- 753 Switzerland: Trans Tech Publications.
- 754 14. Fabbri S, Porcari G, Cugini F, Solzi M, Kamarad J, Arnold Z, Cabassi R, Albertini F. 2014 Co
- 755 and In doped Ni-Mn-Ga magnetic shape memory alloys: a thorough structural, magnetic and
- 756 magnetocaloric study. *Entropy* **16**, 2204–2222. (doi:10.3390/e16042204)
- 757 15. Fabbri S, Albertini F, Paoluzi A, Bolzoni F, Cabassi R, Solzi M, Righi L, Calestani G.
- 758 2009 Reverse magnetostructural transformation in Co-doped NiMnGa multifunctional alloys.
- 759 *Appl. Phys. Lett.* **95**, 022508-1-3. (doi:10.1063/1.3179551)
- 760 16. Fabbri S *et al.* 2011 From direct to inverse giant magnetocaloric effect in Co-doped NiMnGa
- 761 multifunctional alloys. *Acta Mater.* **59**, 412–419. (doi:10.1016/j.actamat.2010.09.059)
- 762 17. Gottschall T, Skokov KP, Frincu B, Gutfleisch O. 2015 Large reversible magnetocaloric effect
- 763 in Ni-Mn-In-Co. *Appl. Phys. Lett.* **106**, 021901-1-4. (doi:10.1063/1.4905371)
- 764 18. Emre B, Yuce S, Stern-Taulats E, Planes A, Fabbri S, Albertini F, Mañosa L. 2013 Large
- 765 reversible entropy change at the inverse magnetocaloric effect in Ni-Co-Mn-Ga-In magnetic
- 766 shape memory alloys. *J. Appl. Phys.* **113**, 213905-1-8. (doi:10.1063/1.4808340)
- 767 19. Niemann R, Diestel A, Backen A, Roessler UK, Behler C, Hahn SM, Wagner F-X, Schultz L,
- 768 Fähler S. 2014 In *Proc. 6th Int. Conf. on Magnetic Refrigeration at Room Temperature (Thermag VI)*,
- 769 Victoria, Canada, 7–10 September 2014.
- 770 20. Diestel A, Niemann R, Schleicher B, Schwabe S, Schultz L, Fähler S. 2015 Field-temperature
- 771 phase diagrams of freestanding and substrate-constrained epitaxial Ni-Mn-Ga-Co films for
- 772 magnetocaloric applications. *J. Appl. Phys.* **118**, 023908-1-11. (doi:10.1063/1.4922358)
- 773 21. Shamberger PJ, Ohuchi FS. 2009 Hysteresis of the martensitic phase transition in
- 774 magnetocaloric-effect NiMnSn alloys. *Phys Rev. B* **79**, 144407-1-9. (doi:10.1103/PhysRevB.79.
- 775 144407)
- 776 22. Titov I, Acet M, Farle M, Gonzalez-Alonso D, Mañosa L, Planes A, Krenke T. 2012 Hysteresis
- 777 effects in the inverse magnetocaloric effect in martensitic Ni-Mn-In and Ni-Mn-Sn. *J. Appl.*
- 778 *Phys.* **112**, 073914-1-5. (doi:10.1063/1.4757425)
- 779 23. Srivastava V, Song YT, Bhatti K, James RD. 2011 The direct conversion of heat to electricity
- 780 using multiferroic alloys. *Adv. Energy Mater.* **1**, 97–104. (doi:10.1002/aenm.201000048)
- 781 24. Cui J *et al.* 2006 Combinatorial search of the thermoelastic shape-memory alloys with
- 782 extremely small hysteresis width. *Nat. Mater.* **5**, 286–290. (doi:10.1038/nmat1593)
- 783 25. Niemann R, Kopeček J, Heczko O, Romberg J, Schultz L, Fähler S, Vives E, Mañosa L, Planes
- 784 A. 2014 Localizing sources of acoustic emission during the martensitic transformation. *Phys.*
- 785 *Rev. B* **89**, 214118-1-11. (doi:10.1103/PhysRevB.89.214118)
- 786 26. Gottschall T, Skokov KP, Burriel R, Gutfleisch O. 2016 On the S(T) diagram of magnetocaloric
- 787 materials with first-order transition: kinetic and cyclic effects of Heusler alloys. *Acta Mater.*
- 788 **107**, 1–8. (doi:10.1016/j.actamat.2016.01.052)
- 789 27. Porcari G, Cugini F, Fabbri S, Pernechele C, Albertini F, Buzzi M, Mangia M, Solzi
- 790 M. 2012 Convergence of direct and indirect methods in the magnetocaloric study of first
- 791 order transformations: the case of Ni-Co-Mn-Ga Heusler alloys. *Phys. Rev. B* **86**, 104432-1-4.
- 792 (doi:10.1103/PhysRevB.86.104432)
- 793 28. Le Bail A, Duroy H, Fourquet JL. 1988 Ab-initio structure determination of LiSbWO₆ by X-ray
- 794 powder diffraction. *Mat. Res. Bull.* **23** 447–452. (doi:10.1016/0025-5408(88)90019-0)
- 795 29. Basso V, Sasso CP, Küpferling MA. 2010 Peltier cells differential calorimeter with kinetic
- correction for the measurement of $c_p(H,T)$ and $\delta s(H,T)$ of magnetocaloric materials. *Rev. Sci.*
- Instrum.* **81**, 113904-1-9. (doi:10.1063/1.3499253)
30. Khovaylo VV *et al.* 2010 Peculiarities of the magnetocaloric properties in Ni-Mn-Sn
- ferromagnetic shape memory alloys. *Phys. Rev. B* **81**, 214406-1-6. (doi:10.1103/PhysRevB.
- 81.214406)

- 796 31. Pecharsky VK, Gschneidner Jr KA. 1999 Magnetocaloric effect from indirect measurements:
797 magnetization and heat capacity. *J. Appl. Phys.* **86**, 565–575. (doi:10.1063/1.370767)
- 798 32. Porcari G, Buzzi M, Cugini F, Pellicelli R, Pernechele C, Caron L, Brück E, Solzi M. 2013 Direct
799 magnetocaloric characterization and simulation of thermomagnetic cycles. *Rev. Sci. Instrum.*
800 **84**, 073907-1-7. (doi:10.1063/1.4815825)
- 801 33. Porcari G, Fabbri S, Pernechele C, Albertini F, Buzzi M, Paoluzi A, Kamarad
802 J, Arnold Z, Solzi M. 2012 Reverse magnetostructural transformation and adiabatic
803 temperature change in Co-, In-substituted Ni-Mn-Ga alloys. *Phys. Rev. B* **85**, 024414-1-7.
804 (doi:10.1103/PhysRevB.85.024414)
- 805 34. Porcari G. 2013 Magnetocaloric effect across first order transformations of energy conversion
806 materials. PhD thesis, ch. 4, University of Parma, Italy.
- 807 35. Pecharsky VK, Gschneidner Jr AK, Pecharsky AO, Tishin AM. 2001 Thermodynamics of the
808 magnetocaloric effect. *Phys. Rev. B* **64**, 144406-1-13. (doi:10.1103/PhysRevB.64.144406)
- 809 36. Guillou F, Porcari G, Yibole H, van Dijk N, Brück E. 2014 Taming the first-order transition in
810 giant magnetocaloric materials. *Adv. Mater.* **26**, 2671–2675. (doi:10.1002/adma.201304788)
- 811
- 812
- 813
- 814
- 815
- 816
- 817
- 818
- 819
- 820
- 821
- 822
- 823
- 824
- 825
- 826
- 827
- 828
- 829
- 830
- 831
- 832
- 833
- 834
- 835
- 836
- 837
- 838
- 839
- 840
- 841
- 842
- 843
- 844
- 845
- 846
- 847
- 848